

Space-Based Observations of Ozone Precursors within California Wildfire Plumes and the Impacts on Ozone- NO_x -VOC Chemistry

Xiaomeng Jin,* Arlene M. Fiore, and Ronald C. Cohen



Cite This: *Environ. Sci. Technol.* 2023, 57, 14648–14660



Read Online

ACCESS |

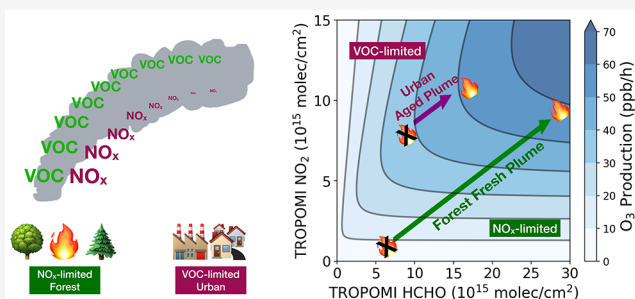
Metrics & More

Article Recommendations

Supporting Information

ABSTRACT: The frequency of wildfires in the western United States has escalated in recent decades. Here we examine the impacts of wildfires on ground-level ozone (O_3) precursors and the O_3 - NO_x -VOC chemistry from the source to downwind urban areas. We use satellite retrievals of nitrogen dioxide (NO_2) and formaldehyde (HCHO, an indicator of VOC) from the Tropospheric Monitoring Instrument (TROPOMI) to track the evolution of O_3 precursors from wildfires over California from 2018 to 2020. We improved these satellite retrievals by updating the *a priori* profiles and explicitly accounting for the effects of smoke aerosols. TROPOMI observations reveal that the extensive and intense fire smoke in 2020 led to an overall increase in statewide annual average HCHO and NO_2 columns by 16% and 9%. The increase in the level of NO_2 offsets the anthropogenic NO_x emission reduction from the COVID-19 lockdown. The enhancement of NO_2 within fire plumes is concentrated near the regions actively burning, whereas the enhancement of HCHO is far-reaching, extending from the source regions to urban areas downwind due to the secondary production of HCHO from longer-lived VOCs such as ethene. Consequently, a larger increase in NO_x occurs in NO_x -limited source regions, while a greater increase in HCHO occurs in VOC-limited urban areas, both contributing to more efficient O_3 production.

KEYWORDS: California wildfires, ozone- NO_x -VOC chemistry, nitrogen dioxide, formaldehyde, volatile organic compounds, remote sensing, TROPOMI



1. INTRODUCTION

Wildfire occurrences have experienced a notable surge over the past few decades in the western United States.^{1,2} The rise in fire-prone weather conditions, attributed to climate change, is expected to further amplify this trend.^{3,4} The annual burned area has increased by more than a factor of 3 over California from 1985 to 2021, largely due to increasing atmospheric aridity caused by warming.⁵ In 2020, California set records for total area burned (1,723,096 ha).⁶ The widespread fire smoke lasted more than 50 days across much of California, reaching 100 days in smoke-prone areas (Figure S1a). The fire season in 2020 led to an unprecedented air quality crisis in the western U.S., contributing about 43% of $\text{PM}_{2.5}$ from August to October.⁷

While the impacts of wildfires on $\text{PM}_{2.5}$ air quality are widely acknowledged, the extent to which biomass burning emissions affect gaseous air pollutants, such as ozone (O_3) and its precursors, remains poorly understood. In California, the national standard for O_3 has been frequently violated.⁸ O_3 production is nonlinearly dependent on the relative availability of two classes of O_3 precursors: oxides of nitrogen ($\text{NO}_x = \text{NO} + \text{NO}_2$) and volatile organic compounds (VOCs). Biomass burning is an important source of both NO_x and VOCs.^{9–12} Model simulation of the impacts of wildfires on O_3 chemistry is

subject to uncertainties with emissions,¹³ plume dynamics,^{14,15} and chemical processes.^{16,17} The in situ measurements from recent Wildfire Experiment for Cloud chemistry, Aerosol absorption, and Nitrogen (WE-CAN) and Fire Influence on Regional to Global Environments and Air Quality experiment (FIREX-AQ) campaigns have advanced our understanding of the impacts of western U.S. wildfires on reactive nitrogen,^{18,19} VOCs,^{11,20} and the O_3 chemistry,^{21,22} but these field campaigns were limited to selected fire episodes and mostly sampled plumes near the source. Over downwind urban areas with high anthropogenic emissions, the impacts of wildfire emissions on O_3 formation will depend on not only the characteristics of fire plumes but also the chemical environment in the recipient areas. In the U.S., anthropogenic NO_x emissions are estimated to have declined by 66% from 2000 to 2020, and anthropogenic VOC emissions have declined by 28%.²³ The nationwide emission control has led to a transition

Received: June 8, 2023

Revised: August 23, 2023

Accepted: August 24, 2023

Published: September 13, 2023



of the O_3 production regime from VOC-limited to NO_x -limited in most U.S. cities except for Los Angeles.²⁴ In-situ measurements have shown evidence that wildfires alter O_3 production regimes near the source,²² and downwind urban areas.²⁵ As anthropogenic emissions continue to decline, while wildfire emissions keep rising, how wildfire emissions of the O_3 precursors, when transported over long distances and mixed with anthropogenic sources, influence the urban O_3 - NO_x -VOC chemistry is an open yet important question.

The full-coverage satellite observations of the O_3 precursors can fill in the spatial gaps of in situ measurements, which enable us to track the evolution of the O_3 precursors from the source to downwind urban areas. Observations of NO_2 tropospheric columns from multiple satellite instruments have been widely used to constrain NO_x emissions from anthropogenic sources and trends in these emissions.^{26–28} Formaldehyde (HCHO) is the second most abundant VOC in wildfire emissions (following acetic acid)¹¹ and is a common intermediate product of the oxidation of most VOCs in the troposphere. Previous studies show that HCHO is a good indicator of organic reactivity when the amount of hydroxyl radicals is sufficient.²⁹ Satellite retrievals of HCHO have been used to constrain VOC emissions from anthropogenic,^{30,31} biogenic sources,^{32,33} as well pyrogenic sources.³⁴ The ratio of HCHO to NO_2 (HCHO/ NO_2) reflects the relative availability total organic reactivity to hydroxyl radicals and NO_x .^{35,36} Studies have used space-based HCHO/ NO_2 to inform the O_3 production regimes.^{24,37–39} Jin et al.²⁴ show that the spatial variability and long-term trends of HCHO/ NO_2 are largely determined by the variations in O_3 precursor emissions from anthropogenic and biogenic sources. Unlike these sources that are persistent and relatively static, the sporadic and transient nature of wildfires makes it challenging to identify their source and chemical evolution over wide spatial and temporal scales. It is not well understood how the transient wildfire emissions influence the O_3 production regimes and the extent to which satellite HCHO/ NO_2 can capture such impacts.

The recently launched TROPOspheric Monitoring Instrument (TROPOMI) offers an unprecedented view of NO_2 and VOC-related species (e.g., HCHO and glyoxal) at fine spatial resolution. TROPOMI has shown an enhanced capability to quantify NO_x emissions over urban areas⁴⁰ and fire plumes.¹² Using TROPOMI HCHO and glyoxal, Alvarado et al.⁴¹ identified long-range transport of HCHO and glyoxal from the 2018 Canadian fires. However, satellite retrievals of NO_2 and HCHO are subject to uncertainties arising from the smoke aerosol effects and biases in the *a priori* profiles.^{34,42,43} While the aerosol optical effects on satellite retrieval of NO_2 are implicitly considered via cloud correction in current operational products,^{44,45} such corrections are less reliable in the presence of heavy aerosol loading from fires.^{42,43} The accuracy of satellite retrievals of NO_2 and HCHO columns largely depends on the *a priori* knowledge of vertical profile shape needed for calculating air mass factor (AMF).^{34,44,46} Improving the spatial resolution of the *a priori* profiles could better resolve the spatial gradients of NO_2 observed from space.^{47–49} Jin et al.¹² applied NASA's fine-resolution ($0.25^\circ \times 0.3125^\circ$) GEOS-CF simulated NO_2 as the *a priori* profile to recalculate AMFs for NO_2 columns near fires, and they showed updating the *a priori* profile could resolve the underestimation of satellite-based NO_x emission factors for fires in previous studies.⁵⁰

Here we improve TROPOMI retrievals of NO_2 and HCHO specifically for fire plumes by updating the *a priori* profiles and

explicitly accounting for the optical effects of smoke aerosols on satellite retrievals. We combine the improved full-coverage TROPOMI retrievals with NOAA's Hazard Mapping System (HMS) smoke product to evaluate the change in NO_2 and HCHO within fire plumes from daily to annual scales. Next, we focus on selected fire plumes and track the evolution of the O_3 precursors as the plume ages. Finally, we assess how the fire-induced changes in the O_3 precursors impact O_3 - NO_x -VOC chemistry from the source to downwind urban areas.

2. MATERIALS AND METHODS

2.1. GEOS-Chem Simulations. We used the GEOS-Chem chemical transport model (v12.7.0),⁵¹ driven by the assimilated meteorological fields from the Goddard Earth Observation System Forward Processing products (GEOS-FP) at $0.25^\circ \times 0.3125^\circ$ spatial resolution. The temporal resolution of GEOS-FP meteorological fields is 3 h for 3-D variables and 1 h for surface quantities and mixing depth. We conducted 3-year (2018 to 2020) nested GEOS-Chem simulations over California and surrounding regions ($27^\circ N$ to $47^\circ N$, $110^\circ W$ to $130^\circ W$).⁵² The boundary conditions are generated from a global simulation at $2^\circ \times 2.5^\circ$ resolution with a 1-year initialization. We used the standard tropospheric chemical scheme that includes detailed NO_x -hydrocarbon-aerosol chemistry.^{53,54} The NEI2011 inventory is used for U.S. anthropogenic emissions and scaled annually based on the national emission trends.²³ We used the biomass burning emissions from the Global Fire Emissions Database (GFED, Version 4.1) inventory,⁵⁵ developed based on Moderate Resolution Imaging Spectroradiometer (MODIS) burned area products.⁵⁶ In GFED, the fuel consumption is derived from biogeochemical models,⁵⁷ and the combustion efficiency is estimated as a function of vegetation attributes and soil moisture.⁵⁵ The emission factors for NMVOCs and NO_x are compiled from lab experiments and in situ measurements, which vary by fuel types.⁵⁸ We distributed 35% biomass burning emissions in the first ten sigma layers above the boundary layer, and the other 65% within the boundary layer.⁵⁹ The standard GEOS-Chem (v12.7.0) does not include biomass burning emissions and chemistry of ethene (C_2H_4), but C_2H_4 is a large contributor to organic reactivity in fire plumes.⁶⁰ We incorporated the chemistry of C_2H_4 following Kwon et al.,⁶¹ and it has been incorporated in standard GEOS-Chem since version 13.3.0. To assess the influence of biomass burning emissions, we ran three additional simulations that (1) turn off total biomass burning emissions (Sim_{NO_Fire}); (2) turn off biomass burning primary emissions of HCHO (Sim_{NO_HCHO}); and (3) turn off biomass burning emissions of C_2H_4 (Sim_{NO_C2H4}).

2.2. TROPOMI Retrievals of HCHO and NO_2 . The TROPOMI instrument aboard the Copernicus Sentinel-5 Precursor satellite provides afternoon observations with a fine spatial resolution ($5.5 \times 3.5 \text{ km}^2$) in the ultraviolet and visible spectra. We used the daily Level-2 TROPOMI retrievals of the NO_2 tropospheric column (version 2.4) and HCHO (version 2) total column densities from May 2018 to December 2020, accessed from NASA's Goddard Earth Sciences Data and Information Services Center (<https://disc.gsfc.nasa.gov>). The retrieval of NO_2 and HCHO columns from radiance data involves three steps.^{44,45} First, the total slant column density is retrieved along the optical path from satellite radiance data. Second, the tropospheric slant column density is derived through the subtraction of the total slant column

density from the stratospheric slant columns.⁴⁴ For HCHO, this step is not needed because the HCHO column in the stratosphere is negligible. The third step is to convert the tropospheric slant column density to vertical column density using AMF. The tropospheric AMF can be expressed as⁶²

$$\text{AMF} = \text{AMF}_G \int_0^1 \omega(\sigma) S(\sigma) d\sigma \quad (1)$$

AMF_G is geometric AMF that is a function of the solar zenith angle and satellite viewing angle.⁶² σ represents the sigma vertical coordinate. $\omega(\sigma)$ is scattering weight that describes the sensitivity of the backscattered spectrum to the abundance of NO_2 or HCHO at each vertical layer. We calculated the scattering weights using the Linearized Discrete Ordinary Radiative Transfer (LIDORT, v2.3),^{63,64} which explicitly account for the aerosol optical effects. The aerosol vertical profiles are obtained from the GEOS-Chem simulations. $S(\sigma)$ is a shape factor that represents the normalized *a priori* vertical profile of NO_2 or HCHO, which is obtained from the GEOS-Chem base simulations at $0.25^\circ \times 0.3125^\circ$. We calculated the $\omega(\sigma)$ for both clear sky and cloudy scenes, and the resulting $\omega(\sigma)$ for partly cloudy scenes is weighted by the radiance-weighted cloud fraction.⁶⁴ We used the cloud pressure and fraction data included in the standard TROPOMI products, which are derived from the TROPOMI O_2 - O_2 cloud product.⁴⁴ The retrieval of clouds implicitly accounts for the aerosol effects, and thus explicit correction of aerosol effects may result in a double-counting of the aerosol impacts on AMF.^{42,65,66} Lin et al.⁴² found that explicitly accounting for aerosol effects in cloud retrieval results in an overall 20% reduction in the cloud radiance fraction. Therefore, we reduced the radiance cloud fraction by 20% in our AMF calculation to reduce the double-counting aerosol effects on the retrievals. We selected TROPOMI HCHO and NO_2 observations that are of good quality that satisfy the following criteria: (1) no processing errors; (2) solar zenith angle $\leq 70^\circ$; (3) cloud radiance fraction (before adjustment) < 0.75 ; (4) surface albedo < 0.2 ; (5) $\text{AMF}/\text{AMF}_G > 0.1$. Overall, our updated TROPOMI NO_2 and HCHO retrievals cover 97% and 88% of the smoky conditions (Figure S1). We interpolated TROPOMI NO_2 and HCHO columns to a regular grid with 0.05° resolution by calculating the area-weighted average.²⁴

2.3. Identification of Fire Plumes. The NOAA's Hazard Mapping System (HMS) smoke product is used to identify potential areas affected by wildfire smoke plumes.⁶⁷ The HMS smoke product is derived based on visual classification of smoke plumes using GOES-16 and GOES-17 ABI true-color imageries.⁶⁸ The HMS smoke product has been applied to evaluate the fire-caused changes in surface $\text{PM}_{2.5}$,^{69,70} O_3 ,⁷¹ and hazardous air pollutants.⁷² We obtained daily HMS smoke products and rasterized them to match the spatial resolutions of gridded TROPOMI NO_2 and HCHO. The rasterized smoke product is used to identify grid cells affected by fire smoke. For each TROPOMI observation within smoke, we define a corresponding background value as the satellite observed NO_2 or HCHO column for those days without smoke at the same location (x, y) and temperature (with less than ± 0.5 C difference) in the same year. We only selected the days with the same temperature to remove the confounding effects of meteorology. We quantified the overall change of NO_2 or HCHO under fire smoke as the change in the annual mean TROPOMI NO_2 and HCHO columns if the observations

under smoky conditions were replaced with the corresponding background values.

The smoke product, however, does not differentiate the smoke plumes from wildfires, agriculture burning, or other sources. As a proof-of-concept evaluation, we applied this method to GEOS-Chem simulated HCHO and NO_2 columns, and calculated the corresponding enhancement of NO_2 and HCHO under fire smoke using the HMS product. We then used a classic model perturbation method that turns off the biomass burning emissions ($\text{Sim}_{\text{No_Fire}}$) in GEOS-Chem, and we estimated the enhancement as the mean relative difference in NO_2 and HCHO between base and $\text{Sim}_{\text{No_Fire}}$ (Figure S2). We found that the smoke-based approach agrees well with the perturbation approach for both NO_2 ($R^2 = 0.99$, $\text{MB} = +3.4\%$, Figure S2a) and HCHO ($R^2 = 0.99$, $\text{MB} = +5.3\%$, Figure S2b). The excellent agreement is due to the strong association between smoke and biomass burning in California.

2.4. Calculation of Plume Age. To track the evolution of the O_3 precursors from source to downwind areas, we identified 2096 plumes from 2018 to 2020 with a clear single fire source. We used the Moderate Resolution Imaging Spectroradiometer (MODIS) Active Fire products (collection 6) to identify the locations of fires in our study region,⁷³ obtained from NASA's Fire Information for Resource Management System.⁷⁴ We grouped fire pixels whose distances are within 20 km as a single fire event, and the center of the fire was calculated as the mean of fire pixel locations weighted by MODIS fire radiative power.¹² For each smoke plume identified from NOAA's HMS product, we searched whether a single fire event occurred within this plume on the same day of the smoke. We did not select the smoke plumes associated with multiple fire locations because such smoke plume is likely a mixture of fresh and aged plumes. Once the fire events are identified, we then used NOAA's Hybrid Single-Particle Lagrangian Integrated Trajectory (HYSPLIT) dispersion model to generate forward dispersion maps starting from the centers of fires,^{75,76} and estimated the plume age as the arrival time of plume for areas identified as smoky areas from HMS smoke product. We used meteorological inputs from North American Regional Reanalysis (NARR) at 36 km resolution.⁷⁷ We ran HYSPLIT at an altitude of 1000 m, which is subject to uncertainties associated with the injection height,¹⁵ especially for extreme fires that can inject large amounts of emissions at high altitudes of the free troposphere.⁷⁸ We ran the model at the same time of day (i.e., 8 AM) for 24 h, which does not account for the actual start time of fires and fire progression, but the resulting plume age should be relatively stable if the wind speed and directions do not vary significantly within hours.

2.5. Analytical Model for O_3 Production. We analyze the relationship between O_3 production and its precursors using a steady-state analytical model that describes a simplified O_3 - NO_x -VOC chemistry.^{79–81} The details of the analytical model are described in the Supporting Information. The input to this analytical model includes near-surface NO , NO_2 , the total organic reactivity (VOCR, defined as sum of the VOC concentration weighted by its reactivity with OH), odd hydrogen radicals (HO_x) production rate (PHO_x) and temperature (T). Given PHO_x , T and $\text{NO}:\text{NO}_2$, the O_3 production rate can be approximated as a function of NO_2 and VOCR, and the sensitivity of O_3 production to precursors can be derived.

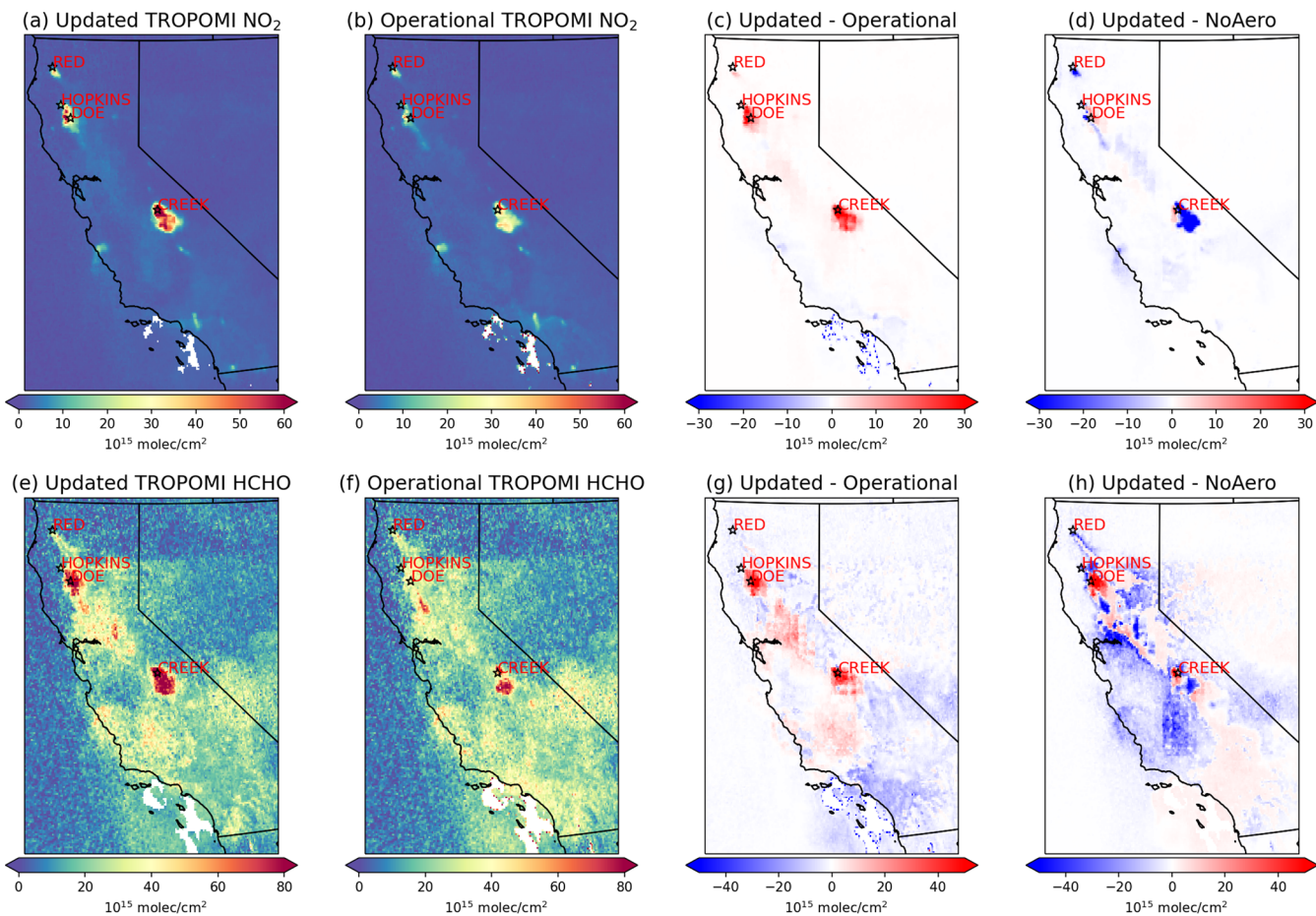


Figure 1. Maps of the updated TROPOMI retrieval of NO_2 tropospheric columns (a) and HCHO columns (e), the operational TROPOMI retrieval of NO_2 tropospheric columns (b) and HCHO columns (f), the difference between the updated and the operational retrievals for NO_2 (c) and HCHO (g), and the difference between the updated TROPOMI retrievals of NO_2 (d) and HCHO (h) with versus without correction for aerosol effects on September 7, 2020 over California. Four big fires that occurred on this day are labeled, and the stars show the center of these big fires.

TROPOMI retrieves tropospheric NO_2 and HCHO columns. The relationship between NO_2 column and surface NO_2 varies with boundary layer height and NO_2 vertical profiles.³⁸ Here we used GEOS-Chem simulations to derive a relationship between the tropospheric NO_2 column and near-surface NO_2 (i.e., effective boundary layer height) and used the model simulated mean $\text{NO}:\text{NO}_2$ fraction to calculate NO . Figure S3a shows the relationship between the GEOS-Chem simulated monthly average tropospheric NO_2 column and the near-surface NO_2 for September 2020, and we found a good correlation ($R^2 = 0.92$, slope = 770 m). For VOCR, we also used GEOS-Chem simulations to derive a relationship between VOCR and HCHO columns. As shown in Figure S3b, HCHO columns are reasonably well correlated with VOCR at the monthly level ($R^2 = 0.81$, slope = 0.5×10^{-15} (molecules/ cm^2) $^{-1} \text{s}^{-1}$). We took the GEOS-Chem simulated PHO_{x} and temperature, from the meteorological data (GEOS-FP) used in GEOS-Chem. We acknowledge that the simple steady-state model lacks details of the O_3-NO_x -VOC chemistry in fire plumes. However, the model provides qualitatively useful information on the sensitivity of O_3 production to its precursors at the scales of TROPOMI observations.^{81,82}

3. RESULTS AND DISCUSSION

3.1. Updated TROPOMI Retrievals Capture HCHO and NO_2 Plumes from Fires. By recalculating the AMF using higher-resolution *a priori* profiles and explicitly accounting for smoke aerosol effects, our updated TROPOMI NO_2 and HCHO retrievals can better detect and quantify the NO_2 and HCHO plumes from fires. For example, Figure 1 shows the TROPOMI tropospheric NO_2 and HCHO columns over California from the new (Figure 1a,e) and the operational products (Figure 1b,f) on September 7, 2020, when several wildfires occurred across California. TROPOMI detects large increases of NO_2 that reach over 80×10^{15} molecules/ cm^2 near the fire center of Creek Fire, over a factor of 3 higher than the NO_2 columns in the city center of Los Angeles (Figure 1a). TROPOMI HCHO columns also peak near the center of Creek Fire (132×10^{15} molecules/ cm^2 , Figure 1e), and such high HCHO columns are rarely observed over California or even globally when no fires are present.⁴⁵ Panels c and g of Figure 1 show the difference in NO_2 and HCHO columns between the updated and the operational standard retrievals. Panels d and h of Figure 1 show the difference if the aerosol effects are not taken into account (i.e., setting the aerosol concentration to be zero when calculating the scattering weight). Compared to the operational standard products (Figure 1b,f), our TROPOMI retrievals with updated *a priori*

vertical profiles and corrections for aerosol effects exhibit larger enhancements of NO_2 and HCHO near fire centers and thus show sharper gradients from the source to downwind areas (Figure 1c,g). For NO_2 , the enhancement is largely due to the finer spatial resolution (nested GEOS-Chem at $0.251^\circ \times 0.3125^\circ$) of the *a priori* profiles than that used in the operational TROPOMI products (TMS-MP at $1^\circ \times 1^\circ$).⁸³ Explicitly accounting for aerosol effects in the satellite retrievals leads to lower NO_2 columns than retrievals that assume no aerosol effects (Figure 1d), consistent with Bouscerez.⁴³ For HCHO , the effects of aerosol vary from fresh to aged smoke, and we found a large fire-to-fire variability. Overall, explicitly accounting for aerosol effects leads to higher HCHO columns near the source, but lower HCHO downwind (Figure 1h), which in combination with higher-resolution *a priori* profiles lead to sharper gradient of HCHO plumes.

3.2. Enhancement of NO_2 within Fire Plumes. While the impacts of fires are generally considered episodic, we found that the long, intense, and widespread fires that occurred in 2020 can impact NO_2 and HCHO across California at seasonal to annual scales. Figure 2 shows the annual mean enhancement

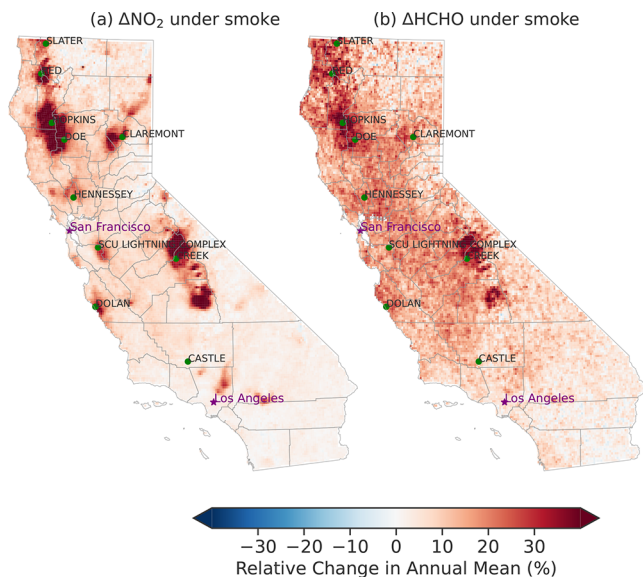


Figure 2. Annual mean relative enhancement of TROPOMI (a) NO_2 and (b) HCHO under smoke in 2020 over California, calculated as the change in annual mean TROPOMI NO_2 or HCHO columns if each observation on smoky days was replaced by the mean of NO_2 or HCHO under clear days at the same temperature. The locations of the major fires are labeled as green dots.

of TROPOMI NO_2 within fire plumes, which is calculated as the change in annual mean TROPOMI NO_2 columns when each observation on smoky days is replaced by the mean of NO_2 on clear days with the same temperature. Half of California had an increase of annual mean NO_2 of at least 5%, and 24% of the state's area had an increase of at least 10%. The largest increases in NO_2 are associated with three big fires: Hopkins, Doe, and Creek Fires (Figure 2), leading to an enhancement of annual mean NO_2 by over 50% near the source. Overall, the wildfires resulted in a statewide annual average NO_2 increase of 9% in 2020 (Figure 3a). During the intensive fire season (August to October), the statewide average of NO_2 increased by 31% under fire smoke (Figure 3a). To get a sense of the magnitude of such increases, the

statewide annual average tropospheric NO_2 has decreased by 3% per year in the past few decades based on OMI observations,^{26,84} which is about a third of the increase in NO_2 due to fire smoke in 2020. The state average NO_2 from April to June was 11% lower in 2020 than in 2019 (Figure 3a), due to the significant reduction of anthropogenic emissions from vehicles during the COVID-19 lockdown.^{85,86} However, fewer fires occurred in 2019 than in 2020, leading to almost no change in NO_2 under fire smoke (Figure 3a). During the fire season from August to October, the state average NO_2 was 32% higher in 2020 than that in 2019. As a result, the statewide annual average of NO_2 in 2020 was 8% higher than that in 2019. If we remove the influences of wildfires (i.e., replacing the NO_2 observations on smoky days with the mean NO_2 on clear days at the same temperature), the annual average NO_2 would be 1% lower in 2020 than in 2019.

Over urban areas away from the fire source, we found that the increases of TROPOMI NO_2 under smoke are less than 5% (Figure 1a), where the plumes are mostly aged, and the base NO_2 is high. Over urban areas away from the fire source, we found that the increases of TROPOMI NO_2 under smoke are less than 5% (Figure 1a). The plumes reaching these areas are mostly aged, and the base NO_2 is high due to anthropogenic emissions. Over urban areas, because of the COVID-19 lockdown, the annual average NO_2 in urban areas was 5% lower in 2020 than in 2019. The monthly average NO_2 was consistently higher in 2019 than in 2020 for all months, except for September (Figure 3c). This suggests that the effects of anthropogenic emission reduction outweighed the effects of fire emissions on NO_x in urban areas, although a stronger reduction of NO_2 by 8% would have occurred in the absence of fires. Ground-based measurements at an urban site downwind from wildfires (Bakersfield, CA) also show negligible increases of NO_x under fire smoke.⁸⁷ Figure 4a shows the relative median enhancement of NO_2 (ΔNO_2) with plume age, calculated from the selected 2096 plumes with clear fire sources. We found that ΔNO_2 is most apparent in fresh plumes (plume age ≤ 3 h), reaching nearly 200% within 1 h, and declines sharply to 27% at 4 h (Figure 4a). In aged plumes older than 6 h, the enhancement of NO_2 is less than 5%. This is consistent with airborne measurements from WE-CAN campaign, which suggest that most of the emitted NO_x from fires are lost within a few hours of plume evolution.¹⁹ The rapid decline of NO_x , however, is not captured in GEOS-Chem, which shows a larger enhancement of NO_2 columns and a slower decline of NO_x with plume age (Figure S4a). Several factors may contribute to the discrepancy between GEOS-Chem and TROPOMI. First, the NO_x emission factor for temperate forest (1.92 g/kg) in GFED is likely to be overestimated, and recent studies suggest a lower NO_x emission factor of 1.36 to 1.56 g/kg.^{12,18} Second, the resolution of GEOS-Chem may be unable to resolve the observed sharp gradient of NO_2 plumes.⁸⁸ Third, the chemical loss of NO_x through the formation of HNO_3 and PAN may be underestimated in GEOS-Chem due to insufficient OH, acetaldehyde (and other larger aldehydes), leading to overestimates of NO_2 enhancement over downwind areas.^{19,89}

3.3. Widespread Increase of HCHO within Fire Plumes. Compared with that of NO_2 , the enhancement of HCHO is far-reaching, extending from forest areas to the downwind cropland and urban regions. Figure 2b shows the overall enhancement of annual mean TROPOMI HCHO columns under fire smoke across California in 2020. More than

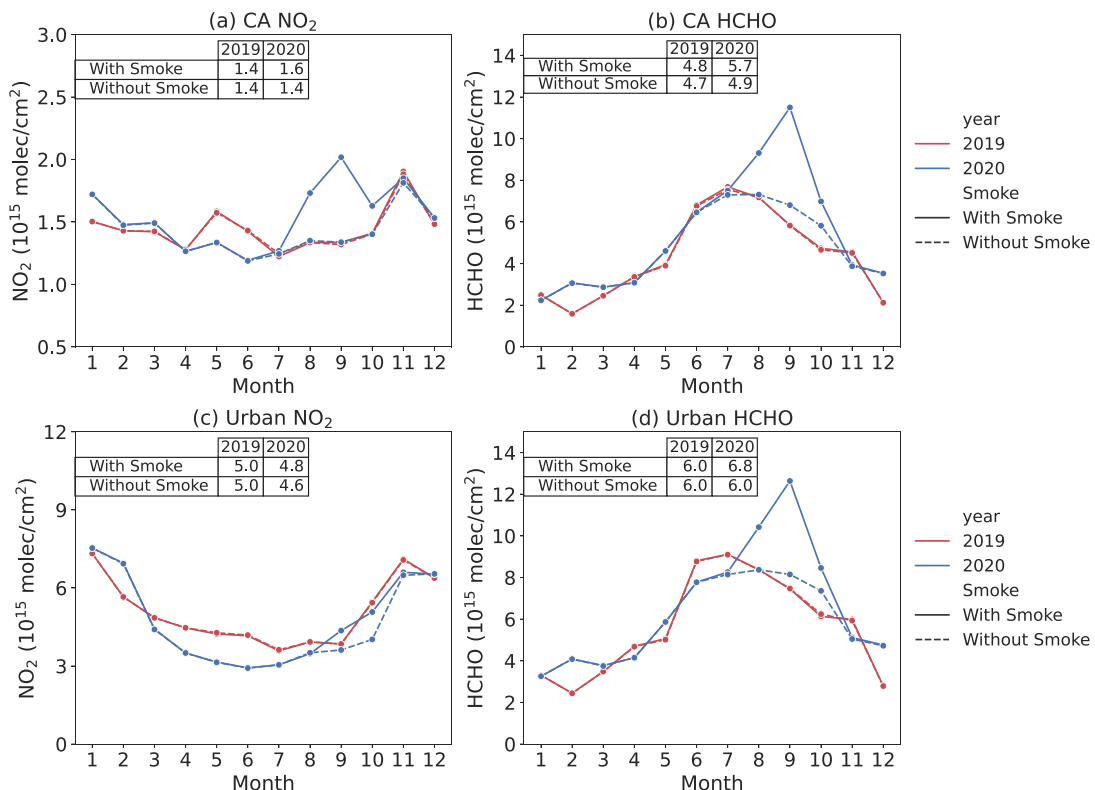


Figure 3. Monthly average TROPOMI NO₂ (left) and HCHO (right) columns over the entire California area (a, b) and the urban areas of California (c, d) in 2019 (red) versus 2020 (blue) with and without fire smoke. The monthly average with smoke is calculated from all observations including smoky and clear days. The average without smoke is calculated by replacing the observations on smoky days with the mean of NO₂ or HCHO on clear days at the same temperature. The table in the upper left corner shows the annual average.

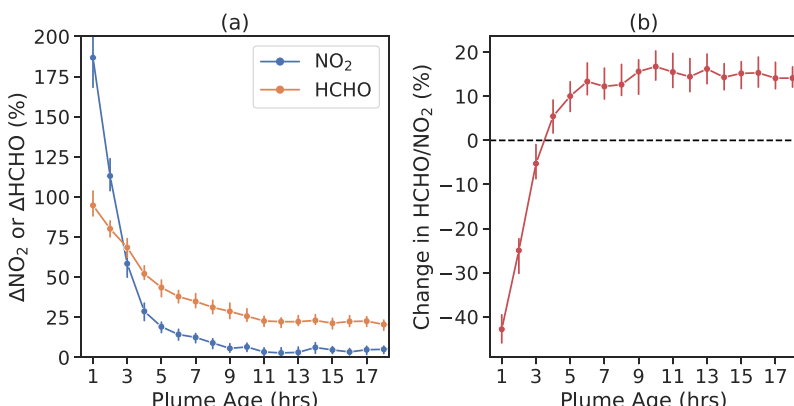


Figure 4. Median relative enhancement of TROPOMI (a) NO₂ (blue) and HCHO (orange) and (b) HCHO/NO₂ as a function with plume age for the 2096 selected plumes from 2018 to 2020. The error bars represent the standard deviation that measures the plume-to-plume variability in the relative enhancement.

80% of the area of California shows an increase of annual mean HCHO by at least 5%, and 59% of the area shows an increase by at least 10%. The maximum increases of HCHO also occurred near the fire centers of Hopkins, Doe, and Creek Fires (~40%). We found a mean enhancement of HCHO of 17% over cropland and 11% over urban areas, which is larger than the mean enhancement of NO₂ (7% over cropland and 3% over urban areas). Overall, TROPOMI observations show a 16% increase in statewide annual average HCHO columns under smoke in 2020, and a 39% increase during the intensive fire season from August to October. The widespread increase in HCHO led to a shift in the seasonal cycle of HCHO: the

peak of HCHO shifted from July 2019 to September 2020 (Figure 3b). The shift in the seasonal cycle is also observed in downwind urban areas (Figure 3d).

Next, we focused on selected 2096 plumes with clear fire sources and track the evolution of HCHO from source to downwind. In contrast to the TROPOMI NO₂ which declines quickly, ΔHCHO, on the other hand, declines more slowly with plume age, from around 90% at 1 h to 30% at 6 h (Figure 4a). Overall, ΔHCHO is lower than ΔNO₂ in plumes younger than 3 h but higher than ΔNO₂ in plumes older than 3 h (Figure 4a). We observed a consistent positive ΔHCHO of more than 20% in the aged plumes older than 6 h (Figure 4a).

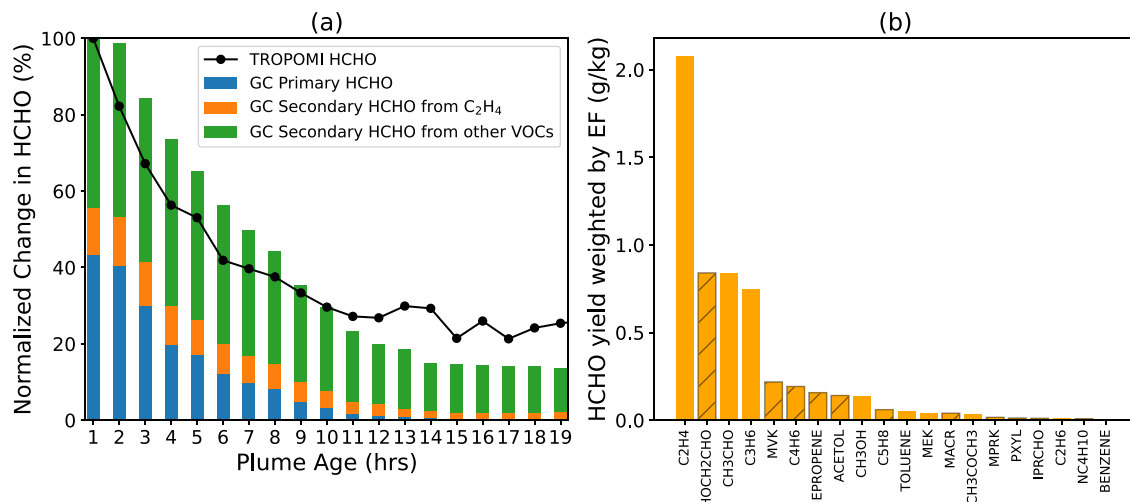


Figure 5. (a) GEOS-Chem simulated and TROPOMI observed ΔHCHO with plume age normalized by the ΔHCHO at the fire center. (b) 24-h HCHO yield from oxidation of VOCs weighted by the corresponding emission factors reported in Permar et al.¹¹ Here we show only the top 20 VOC species. Bars with hatches represent VOC species not included in the biomass burning emission inventory in GEOS-Chem.

TROPOMI observations of the 2018 Canadian fires also show enhancement of HCHO for up to 1500 km.⁴¹ Consistent with our findings, in situ measurements of VOCs in an urban area 60 km downwind from the October 2017 northern California wildfires also show enhancement of HCHO and other secondary VOCs (e.g., acetaldehyde, maleic anhydride) in the aged plumes.²⁵ Using airborne measurements of HCHO and VOCs from the FIREX-AQ field campaign, Liao et al.²⁰ found the dilution-normalized HCHO increases with plume age in the majority of the plumes sampled.

Since the lifetime of HCHO in the troposphere is generally within several hours,²⁹ the widespread enhancement of HCHO in aged plumes must be due to the secondary production of HCHO from the oxidation of VOCs as the plumes age and are transported. We used GEOS-Chem simulations to evaluate the contributions of primary and secondary sources on the evolution of HCHO along fire plumes. We sampled GEOS-Chem modeled HCHO columns consistently for those plumes with clear fire centers. GEOS-Chem and TROPOMI observations show reasonably good agreement in terms of the absolute enhancement of HCHO columns within fire plumes (Figure S4b). Figure 5a shows the GEOS-Chem simulated and TROPOMI observed ΔHCHO with plume age normalized by ΔHCHO at the fire center. We focused on the normalized ΔHCHO rather than the absolute ΔHCHO because the absolute ΔHCHO is largely affected by the primary biomass burning emissions, but here we are interested in the evolution of HCHO. We found that GEOS-Chem can capture the observed evolution of HCHO with plume age, both suggesting that ΔHCHO is reduced to 20% after 10 h. We estimated that the contribution from primary sources is the difference between Base and Sim_{No_HCHO} in GEOS-Chem, and the contribution from secondary sources is the difference between Sim_{No_HCHO} and Sim_{No_Fire}. These simulations show that HCHO enhancement in aged plumes is mainly due to the secondary production of HCHO from the oxidation of other VOCs. Primary emissions of HCHO contribute about 40% of the total HCHO enhancement in fresh plumes (<3 h), which reduces to 20% at 6 h. In plumes older than 10 h, more than 95% of the HCHO enhancement is due to secondary production. This is consistent with the findings from the

FIREX-AQ campaign, which suggest that the secondary production of HCHO via oxidation of VOCs is the main driver of the sustained enhancement of HCHO from fires.²⁰

To evaluate which VOC species lead to the HCHO enhancement in aged plumes, we calculated the HCHO yield of HCHO-producing VOC species identified in fire plumes during the WE-CAN wildfire campaign.¹¹ The HCHO yield is calculated using Framework for 0-D Atmospheric Modeling (F0AM, version 4.1) with the Master Chemical Mechanism (version 3.3.1, Supporting Information).^{90–93} Accounting for the variations of the emission factors of each VOC, we multiplied the HCHO yield with the emission factors reported in Permar et al.,¹¹ which represents the amount of HCHO produced per unit of mass burned. Figure 5b shows the top 20 contributors to secondary HCHO. We found that C₂H₄ is the largest contributor to secondary HCHO, which has both a high HCHO yield and a high emission factor. Oxidation of C₂H₄ slowly produces HCHO with peak production around 10 h downwind (Figure S5). We evaluated the difference between Base and Sim_{No_C2H4} as the contribution from biomass burning C₂H₄. We found that fire C₂H₄ contributes about 15% of HCHO enhancement in aged plumes, but its contribution decreases with plume age, suggesting that GEOS-Chem may underestimate the slow production of HCHO from C₂H₄ in aged plumes. It should be noted that the biomass burning emission inventory in GEOS-Chem includes 16 VOC species. We found that GEOS-Chem does not include 6 of the 10 VOC species that have the largest emission factor weighted HCHO yield (Figure 5b). Indeed, we found that GEOS-Chem tends to underestimate the HCHO enhancement in plumes older than 10 h (Figure 5a), which is likely due to the contribution from those missing fire VOCs, or inaccurate representation of the later-generation VOC degradation products. Expansion of VOC species in GEOS-Chem could improve the representation of VOC reactivity,⁶⁰ and it is expected that the relative contributions of primary emissions to HCHO will be even smaller if we include more HCHO precursors. Hundreds of VOC species are known to be present in fire plumes, and many of them remain unidentified.¹¹ Further identification, specification, and quantification of fire VOCs from field measurements, and improvement of model representations of fire

VOCs are needed to further understand secondary production of HCHO. Also, while we focus on the ozone- NO_x -VOC chemistry, it should also be noted that HCHO near the surface is a hazardous air pollutant that is a cause of lung and nasopharyngeal cancer.⁹⁴ The widespread increase of HCHO within wildfire plumes will negatively affect human health in addition to the known health impacts of smoke aerosols.⁷²

3.4. Effects of Fire NO_x and VOC Emissions on O_3 Production.

O_3 is nonlinearly dependent on the relative availability of NO_x versus VOCs. We evaluated the changes in the ratio of TROPOMI HCHO to NO_2 (HCHO/NO_2) within fire plumes as an indicator of the effects of fire emissions on the relative availability of NO_x versus VOCs.^{24,38,39,95} Figure 4b shows the overall median changes of TROPOMI HCHO/ NO_2 within fire plumes ($\Delta\text{HCHO}/\text{NO}_2$) with plume age. We found a decrease of HCHO/NO_2 within fresh fire plumes (plume age ≤ 3 h), meaning that the increase of NO_2 outweighs the increase of HCHO. In aged plumes older than 3 h, an increase of HCHO/NO_2 is found, meaning that the increase of HCHO outweighs that of NO_2 .

Under smoke-free conditions, O_3 production is generally NO_x -limited in forest regions but tends to be VOC-limited (or NO_x -saturated) over urban areas with high anthropogenic NO_x emissions. Figure 6 shows an isopleth of O_3 production as a function of NO_2 and HCHO columns based on the steady-state analytical model (Section 2.5 and Supporting Information). At low NO_2 concentrations or high HCHO/NO_2 (i.e., NO_x -limited regime), O_3 production increases with NO_2 , but it is insensitive to VOC emissions. Fire-induced changes in NO_2

are mostly concentrated in the NO_x -limited forest regions, where the O_3 production per NO_x (i.e., O_3 production efficiency) is high.^{97,98} That is, for the same amount of increase in NO_x , fire NO_x in forests is more efficient at producing O_3 than anthropogenic NO_x in urban areas: an increase of 10^{15} molecules/cm² in tropospheric column NO_2 leads to a +7 ppb/h increase in O_3 production near the fire, but a decrease in O_3 production of -0.1 ppb/h in urban Los Angeles. In fresh plumes, both HCHO and NO_2 increase, and overall O_3 production remains in the NO_x -limited regime in the early afternoon (Figure 6), consistent with findings from the FIREX-AQ campaign.^{21,22} In the NO_x -limited regime, a small decrease of HCHO/NO_2 is associated with more efficient O_3 production,²⁴ but a regime transition from NO_x -limited to a NO_x -saturated regime can be found at the plume center,⁹⁹ other times of the day,²² or extreme fires with substantial emissions of NO_x ,⁷⁸ at which O_3 production is inhibited by NO_x .

At high NO_2 concentrations (i.e., NO_x -saturated or VOC-limited regime), which mostly occurs in urban areas with high anthropogenic NO_x emissions, O_3 production increases with increasing HCHO but decreases with NO_2 due to the NO_x suppression of hydroxyl radicals. The fire plumes that reach urban areas are mostly aged, where we found an increase of HCHO, which enhances O_3 production. For example, the mean HCHO increased from 10×10^{15} molecules/cm² to 14×10^{15} molecules/cm² over Los Angeles in September 2020, leading to an increase in O_3 production by 7 ppb/h based on the steady-state model (Figure 6). Because of the emission controls from power plants and vehicles, the NO_2 level has decreased substantially over Los Angeles, which makes O_3 production less sensitive to VOCs.²⁴ The same amount of HCHO increase would have led to a larger increase in O_3 production if NO_2 in Los Angeles was at the 2006–2010 mixing ratios. In other urban areas where the NO_2 level is lower, the O_3 production regime has made the transition toward the NO_x -limited regime in 2020, meaning that O_3 production is almost insensitive to VOCs.²⁴ For example, the mean NO_2 over urban areas of San Bernardino is 6×10^{15} molecules/cm² without smoke, and the increase of HCHO within fire plumes ($+3 \times 10^{15}$ molecules/cm²) leads to an increase of O_3 production by 2 ppbv/h. For other urban areas, the mean NO_2 is 4×10^{15} molecules/cm², and the enhancement of HCHO within fire plumes leads to an increase of O_3 production by less than 1 ppbv/h. The increase of HCHO/NO_2 within fire plumes further facilitates the transition from the NO_x -saturated to the NO_x -limited regime in urban areas. Similarly, Liang et al.²⁵ found the increase of fire-related VOCs has shifted the O_3 production toward a NO_x -limited regime during the 2017 wildfire season in the San Francisco Bay Area.

To summarize, using updated TROPOMI retrievals of NO_2 and HCHO, we found that wildfires have large impacts on the production of O_3 precursors, leading to an overall increase in the statewide annual average HCHO and NO_2 columns by 16% and 9% in 2020. The enhancement of NO_2 within fire plumes is concentrated in the NO_x -limited source regions, whereas the enhancement of HCHO is far-reaching, extending from the source regions to VOC-limited urban areas downwind, both contributing to more efficient production of O_3 . While the emissions of O_3 precursors from wildfires increase O_3 production, the overall impacts of wildfires on O_3 concentration are more complicated. Field studies show a large

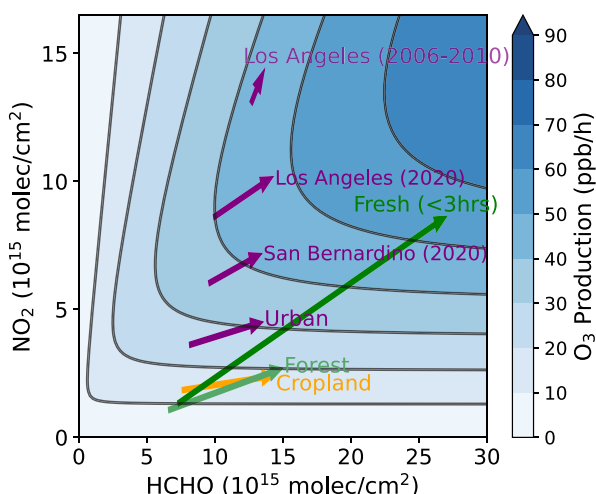


Figure 6. Isopleth of the O_3 production rate (ppb/h) as a function of NO_2 and HCHO columns based on a steady-state analytical model. The arrows represent the TROPOMI observed change of the NO_2 and HCHO columns within fire plumes in September 2020 for two cities (Los Angeles and San Bernardino) and three land cover types (urban, forest, cropland). The land cover type is classified using MODIS land cover product.⁹⁶ The arrowhead is the mean NO_2 and HCHO on smoky days, and the arrow tail is the mean NO_2 and HCHO on clear days at the same temperature (background value). O_3 production is calculated from the steady-state simple model by varying the NO_x and VOC reactivities for given values PHO_{x} , $\text{NO}:\text{NO}_2$, temperature. PHO_{x} , $\text{NO}:\text{NO}_2$ are assumed to be constant as the monthly average GEOS-Chem simulated PHO_{x} , $\text{NO}:\text{NO}_2$ fraction for California in September 2020. The relationships between the NO_2 column and NO_2 , VOC reactivity, and HCHO are derived from GEOS-Chem simulations (Figure S3).

variability of O₃ chemistry from the center to the edge of the fire plume.^{21,100} The smoke aerosols from fires are expected to decrease O₃ production by reducing the photolysis rates.¹⁰¹ The uptake of HO₂ radicals onto the aerosol surfaces is proposed as a sink of radicals under heavy aerosol loading,¹⁰² but the photolysis of HONO and HCHO from fires produces additional HO_x.^{22,103} While our steady-state model does not account for all of these effects downwind in cities, we expect that the increase in HCHO dominates and that the results presented herein illustrate key features of the urban chemistry of remote fires. Further investigations of the effects of precursor emissions and smoke aerosols on O₃ production and the resulting impacts on the spatiotemporal variability of O₃ are warranted.

Here we intend to elucidate the regional-scale impacts of wildfire smoke on the O₃-NO_x-VOC chemistry by aggregating observations from a large number of fire episodes. However, TROPOMI observations for individual fire episodes are subject to large uncertainties, and the resolution of TROPOMI is unable to resolve the spatial variability of the O₃ chemistry within fire plumes. We use the *a priori* profiles from GEOS-Chem simulations at 0.25° × 0.3125° resolution, which significantly reduces the resolution-dependent uncertainties in the operational products that use global simulations at 1° resolution,^{83,88} but improving the spatial resolution of *a priori* to a resolution of 0.1° or finer could help further resolve the spatial gradients of NO₂ and HCHO within fire plumes.^{83,88} The fire injection height is assumed to be constant for all fires in GEOS-Chem and HYSPLIT, which is a major source of uncertainty that could lead to errors in simulating the smoke dispersion, especially for extreme fires.¹⁰⁴ Also, satellite retrievals of NO₂ and HCHO are subject to large uncertainty in cloudy areas,^{42,43,45} and future work that explicitly accounts for the aerosol effects in cloud retrieval could help reduce such uncertainty.^{42,65} Evaluation of TROPOMI retrievals and GEOS-Chem simulated *a priori* profiles with airborne measurements from field campaigns (e.g., WE-CAN, FIREX-AQ) and ground-based MAX-DOAS measurements is warranted to better understand and quantify the uncertainties of TROPOMI observations under fire smoke. Future work should conduct a more detailed evaluation of reactive nitrogen partitioning and VOC composition in GEOS-Chem to determine the mechanisms affecting the formation and loss of NO₂ and HCHO downwind of fires. In addition, the daily snapshot from TROPOMI does not resolve the time-of-day dependence of O₃ chemistry in fire plumes.²² The recently launched TEMPO instrument on the geostationary orbit will provide continuous observations of O₃ precursors throughout the day,¹⁰⁵ allowing more detailed time evolution of fire plumes to be observed.

ASSOCIATED CONTENT

Supporting Information

The Supporting Information is available free of charge at <https://pubs.acs.org/doi/10.1021/acs.est.3c04411>.

Descriptions of the steady state model for O₃ production; calculation of HCHO yield from oxidation of VOCs; Figure S1, number of smoke days in 2020 over California identified from NOAA's HMS products and number of days with valid TROPOMI observations under smoke; Figure S2, comparison of the GEOS-Chem simulated changes in (a) NO₂ and (b) HCHO

under fire smoke that uses smoke-based methods versus model perturbation approach; Figure S3, scatterplots between (a) GEOS-Chem simulated tropospheric NO₂ column vs surface NO₂ number density; (b) GEOS-Chem simulated HCHO column density vs near-surface VOC reactivity; Figure S4, absolute enhancement of NO₂ and HCHO from TROPOMI observations versus GEOS-Chem simulations (blue) as a function with plume age; Figure S5, production of HCHO from oxidation of different VOCs with time ([PDF](#))

AUTHOR INFORMATION

Corresponding Author

Xiaomeng Jin – Department of Environmental Sciences, Rutgers, The State University of New Jersey, New Brunswick, New Jersey 08901, United States;  orcid.org/0000-0002-6895-8464; Email: xiaomeng.jin@rutgers.edu

Authors

Arlene M. Fiore – Department of Earth, Atmospheric and Planetary Sciences, Massachusetts Institute of Technology, Cambridge, Massachusetts 02139, United States

Ronald C. Cohen – Department of Chemistry and Department of Earth and Planetary Sciences, University of California Berkeley, Berkeley, California 94720, United States;  orcid.org/0000-0001-6617-7691

Complete contact information is available at:

<https://pubs.acs.org/10.1021/acs.est.3c04411>

Author Contributions

X.J.: Conceptualization, Methodology, Formal analysis, Data Curation, Visualization, Writing - Original Draft. A.M.F.: Writing - Review & Editing, Computing Resources. R.C.C.: Funding acquisition, Writing - Review & Editing, Computing Resources. All authors have given approval to the final version of the manuscript.

Notes

The authors declare no competing financial interest.

ACKNOWLEDGMENTS

This study was supported by NOAA Climate Program Office's Atmospheric Chemistry, Carbon Cycle, and Climate program, grant number NA22OAR4310199. This research used the computational cluster resource provided by the Office of Advanced Research Computing (OARC) at Rutgers, The State University of New Jersey, the Berkeley Research Computing program at the University of California, Berkeley and Columbia University's Shared Research Computing Facility project. We would like to thank Kelvin Bates from NOAA's Chemical Sciences Laboratory for helping implement C₂H₄ chemistry in GEOS-Chem and Jin-tai Lin from Peking University for useful discussions on accounting for aerosol effects in TROPOMI retrievals.

REFERENCES

- (1) Westerling, A. L.; Hidalgo, H. G.; Cayan, D. R.; Swetnam, T. W. Warming and Earlier Spring Increase Western US Forest Wildfire Activity. *Science* **2006**, *313* (5789), 940–943.
- (2) Abatzoglou, J. T.; Battisti, D. S.; Williams, A. P.; Hansen, W. D.; Harvey, B. J.; Kolden, C. A. Projected Increases in Western US Forest Fire despite Growing Fuel Constraints. *Commun. Earth Environ* **2021**, *2* (1), 227.

- (3) Abatzoglou, J. T.; Williams, A. P. Impact of Anthropogenic Climate Change on Wildfire across Western US Forests. *Proc. Natl. Acad. Sci. U. S. A.* **2016**, *113* (42), 11770–11775.
- (4) Williams, A. P.; Abatzoglou, J. T.; Gershunov, A.; Guzman-Morales, J.; Bishop, D. A.; Balch, J. K.; Lettenmaier, D. P. Observed Impacts of Anthropogenic Climate Change on Wildfire in California. *Earth's Future* **2019**, *7* (8), 892–910.
- (5) Juang, C. S.; Williams, A. P.; Abatzoglou, J. T.; Balch, J. K.; Hurteau, M. D.; Moritz, M. A. Rapid Growth of Large Forest Fires Drives the Exponential Response of Annual Forest-Fire Area to Aridity in the Western United States. *Geophys. Res. Lett.* **2022**, *49* (5), No. e2021GL097131.
- (6) Porter, T.; Crowfoot, W.; Newsom, G. 2020 Wildfire Activity Statistics; CA.gov, 2020. <https://www.fire.ca.gov/our-impact/statistics> (accessed 2023-05-12).
- (7) Li, Y.; Tong, D.; Ma, S.; Zhang, X.; Kondragunta, S.; Li, F.; Saylor, R. Dominance of Wildfires Impact on Air Quality Exceedances During the 2020 Record-Breaking Wildfire Season in the United States. *Geophys. Res. Lett.* **2021**, *48* (21).
- (8) U.S. EPA. California Nonattainment/Maintenance Status for Each County by Year for All Criteria Pollutants. https://www3.epa.gov/airquality/greenbook/anayo_ca.html (accessed 2023-05-12).
- (9) Andreae, M. O.; Merlet, P. Emission of Trace Gases and Aerosols from Biomass Burning. *Global Biogeochemical Cycles* **2001**, *15* (4), 955–966.
- (10) Crutzen, P. J.; Andreae, M. O. Biomass Burning in the Tropics: Impact on Atmospheric Chemistry and Biogeochemical Cycles. *Science* **1990**, *250*, 1669–1678.
- (11) Permar, W.; Wang, Q.; Selimovic, V.; Wielgasz, C.; Yokelson, R. J.; Hornbrook, R. S.; Hills, A. J.; Apel, E. C.; Ku, I.; Zhou, Y.; Sive, B. C.; Sullivan, A. P.; Collett, J. L.; Campos, T. L.; Palm, B. B.; Peng, Q.; Thornton, J. A.; Garofalo, L. A.; Farmer, D. K.; Kreidenweis, S. M.; Levin, E. J. T.; DeMott, P. J.; Flocke, F.; Fischer, E. V.; Hu, L. Emissions of Trace Organic Gases From Western U.S. Wildfires Based on WE-CAN Aircraft Measurements. *J. Geophys. Res. Atmospheres* **2021**, *126* (11). DOI: 10.1029/2020JD033838.
- (12) Jin, X.; Zhu, Q.; Cohen, R. C. Direct Estimates of Biomass Burning NO_x Emissions and Lifetimes Using Daily Observations from TROPOMI. *Atmos. Chem. Phys.* **2021**, *21* (20), 15569–15587.
- (13) Andreae, M. O. Emission of Trace Gases and Aerosols from Biomass Burning – an Updated Assessment. *Atmospheric Chemistry and Physics* **2019**, *19* (13), 8523–8546.
- (14) Li, Y.; Tong, D.; Ma, S.; Freitas, S. R.; Ahmadov, R.; Sofiev, M.; Zhang, X.; Kondragunta, S.; Kahn, R.; Tang, Y.; Baker, B.; Campbell, P.; Saylor, R.; Grell, G.; Li, F. Impacts of Estimated Plume Rise on PM_{2.5} Exceedance Prediction during Extreme Wildfire Events: A Comparison of Three Schemes (Briggs, Freitas, and Sofiev). *Atmos. Chem. Phys.* **2023**, *23* (5), 3083–3101.
- (15) Ye, X.; Saide, P. E.; Hair, J.; Fenn, M.; Shingler, T.; Soja, A.; Gargulinski, E.; Wiggins, E. Assessing Vertical Allocation of Wildfire Smoke Emissions Using Observational Constraints From Airborne Lidar in the Western U.S. *J. Geophys. Res. Atmospheres* **2022**, *127* (21), No. e2022JD036808.
- (16) Young, P. J.; Naik, V.; Fiore, A. M.; Gaudel, A.; Guo, J.; Lin, M. Y.; Neu, J. L.; Parrish, D. D.; Rieder, H. E.; Schnell, J. L.; Tilmes, S.; Wild, O.; Zhang, L.; Ziemke, J.; Brandt, J.; Delclos, A.; Doherty, R. M.; Geels, C.; Hegglin, M. I.; Hu, L.; Im, U.; Kumar, R.; Luhar, A.; Murray, L.; Plummer, D.; Rodriguez, J.; Saiz-Lopez, A.; Schultz, M. G.; Woodhouse, M. T.; Zeng, G. Tropospheric Ozone Assessment Report: Assessment of Global-Scale Model Performance for Global and Regional Ozone Distributions, Variability, and Trends. *Elem. Sci. Anth.* **2018**, *6* (1). DOI: 10.1525/elementa.265.
- (17) Zhang, L.; Jacob, D. J.; Kopacz, M.; Henze, D. K.; Singh, K.; Jaffe, D. A. Intercontinental Source Attribution of Ozone Pollution at Western U.S. Sites Using an Adjoint Method. *Geophys. Res. Lett.* **2009**, *36* (11), L11810–5.
- (18) Lindaas, J.; Pollack, I. B.; Garofalo, L. A.; Pothier, M. A.; Farmer, D. K.; Kreidenweis, S. M.; Campos, T. L.; Flocke, F.; Weinheimer, A. J.; Montzka, D. D.; Tyndall, G. S.; Palm, B. B.; Peng, Q.; Thornton, J. A.; Permar, W.; Wielgasz, C.; Hu, L.; Ottmar, R. D.; Restaino, J. C.; Hudak, A. T.; Ku, I.; Zhou, Y.; Sive, B. C.; Sullivan, A.; Collett, J. L.; Fischer, E. V. Emissions of Reactive Nitrogen From Western U.S. Wildfires During Summer 2018. *J. Geophys. Res. Atmospheres* **2021**, *126* (2). DOI: 10.1029/2020JD032657.
- (19) Peng, Q.; Palm, B. B.; Fredrickson, C. D.; Lee, B. H.; Hall, S. R.; Ullmann, K.; Campos, T.; Weinheimer, A. J.; Apel, E. C.; Flocke, F.; Permar, W.; Hu, L.; Garofalo, L. A.; Pothier, M. A.; Farmer, D. K.; Ku, I.-T.; Sullivan, A. P.; Collett, J. L.; Fischer, E.; Thornton, J. A. Observations and Modeling of NO_x Photochemistry and Fate in Fresh Wildfire Plumes. *ACS Earth Space Chem.* **2021**, *5* (10), 2652–2667.
- (20) Liao, J.; Wolfe, G. M.; Hannun, R. A.; St. Clair, J. M.; Hanisco, T. F.; Gilman, J. B.; Lamplugh, A.; Selimovic, V.; Diskin, G. S.; Nowak, J. B.; Halliday, H. S.; DiGangi, J. P.; Hall, S. R.; Ullmann, K.; Holmes, C. D.; Fite, C. H.; Agastra, A.; Ryerson, T. B.; Peischl, J.; Bourgeois, I.; Warneke, C.; Coggon, M. M.; Gkatzelis, G. I.; Sekimoto, K.; Fried, A.; Richter, D.; Weibring, P.; Apel, E. C.; Hornbrook, R. S.; Brown, S. S.; Womack, C. C.; Robinson, M. A.; Washenfelder, R. A.; Veres, P. R.; Neuman, J. A. Formaldehyde Evolution in US Wildfire Plumes during the Fire Influence on Regional to Global Environments and Air Quality Experiment (FIREX-AQ). *Atmos. Chem. Phys.* **2021**, *21* (24), 18319–18331.
- (21) Xu, L.; Crounse, J. D.; Vasquez, K. T.; Allen, H.; Wennberg, P. O.; Bourgeois, I.; Brown, S. S.; Campuzano-Jost, P.; Coggon, M. M.; Crawford, J. H.; DiGangi, J. P.; Diskin, G. S.; Fried, A.; Gargulinski, E. M.; Gilman, J. B.; Gkatzelis, G. I.; Guo, H.; Hair, J. W.; Hall, S. R.; Halliday, H. A.; Hanisco, T. F.; Hannun, R. A.; Holmes, C. D.; Huey, L. G.; Jimenez, J. L.; Lamplugh, A.; Lee, Y. R.; Liao, J.; Lindaas, J.; Neuman, J. A.; Nowak, J. B.; Peischl, J.; Peterson, D. A.; Piel, F.; Richter, D.; Rickly, P. S.; Robinson, M. A.; Rollins, A. W.; Ryerson, T. B.; Sekimoto, K.; Selimovic, V.; Shingler, T.; Soja, A. J.; St. Clair, J. M.; Tanner, D. J.; Ullmann, K.; Veres, P. R.; Walega, J.; Warneke, C.; Washenfelder, R. A.; Weibring, P.; Wisthaler, A.; Wolfe, G. M.; Womack, C. C.; Yokelson, R. J. Ozone Chemistry in Western U.S. Wildfire Plumes. *Sci. Adv.* **2021**, *7* (50), No. eabl3648.
- (22) Robinson, M. A.; Decker, Z. C. J.; Barsanti, K. C.; Coggon, M. M.; Flocke, F. M.; Franchin, A.; Fredrickson, C. D.; Gilman, J. B.; Gkatzelis, G. I.; Holmes, C. D.; Lamplugh, A.; Lavi, A.; Middlebrook, A. M.; Montzka, D. M.; Palm, B. B.; Peischl, J.; Pierce, B.; Schwantes, R. H.; Sekimoto, K.; Selimovic, V.; Tyndall, G. S.; Thornton, J. A.; Van Rooy, P.; Warneke, C.; Weinheimer, A. J.; Brown, S. S. Variability and Time of Day Dependence of Ozone Photochemistry in Western Wildfire Plumes. *Environ. Sci. Technol.* **2021**, *55* (15), 10280–10290.
- (23) U.S. EPA. Air Pollutant Emissions Trends Data. <https://www.epa.gov/air-emissions-inventories/air-pollutant-emissions-trends-data> (accessed 2023-05-12).
- (24) Jin, X.; Fiore, A.; Boersma, K. F.; Smedt, I. D.; Valin, L. Inferring Changes in Summertime Surface Ozone–NO_x–VOC Chemistry over U.S. Urban Areas from Two Decades of Satellite and Ground-Based Observations. *Environ. Sci. Technol.* **2020**, *54* (11), 6518–6529.
- (25) Liang, Y.; Weber, R. J.; Misztal, P. K.; Jen, C. N.; Goldstein, A. H. Aging of Volatile Organic Compounds in October 2017 Northern California Wildfire Plumes. *Environ. Sci. Technol.* **2022**, *56* (3), 1557–1567.
- (26) Duncan, B. N.; Lamsal, L. N.; Thompson, A. M.; Yoshida, Y.; Lu, Z.; Streets, D. G.; Hurwitz, M. M.; Pickering, K. E. A Space-Based, High-Resolution View of Notable Changes in Urban NO_x Pollution around the World (2005–2014). *Journal of Geophysical Research: Atmospheres* **2016**, *121* (2), 976–996.
- (27) Liu, F.; Zhang, Q.; van der A, R. J.; Zheng, B.; Tong, D.; Yan, L.; Zheng, Y.; He, K. Recent Reduction in NO_x emissions over China: Synthesis of Satellite Observations and Emission Inventories. *Environmental Research Letters* **2016**, *11* (11), 114002–114010.
- (28) Lu, Z.; Streets, D. G.; de Foy, B.; Lamsal, L. N.; Duncan, B. N.; Xing, J. Emissions of Nitrogen Oxides from US Urban Areas: Estimation from Ozone Monitoring Instrument Retrievals for 2005–2014. *Atmospheric Chemistry and Physics* **2015**, *15* (18), 10367–10383.

- (29) Valin, L. C.; Fiore, A. M.; Chance, K.; Abad, G. G. The Role of OH Production in Interpreting the Variability of CH₂O Columns in the Southeast U.S. *J. Geophys. Res. Atmospheres* **2016**, *121* (1), 478–493.
- (30) Zhu, L.; Jacob, D. J.; Mickley, L. J.; Marais, E. A.; Cohan, D. S.; Yoshida, Y.; Duncan, B. N.; Abad, G. G.; Chance, K. V. Anthropogenic Emissions of Highly Reactive Volatile Organic Compounds in Eastern Texas Inferred from Oversampling of Satellite (OMI) Measurements of HCHO Columns. *Environmental Research Letters* **2014**, *9* (11), 114004–114008.
- (31) Cao, H.; Fu, T.-M.; Zhang, L.; Henze, D. K.; Miller, C. C.; Lerot, C.; Abad, G. G.; De Smedt, I.; Zhang, Q.; van Roozendael, M.; Hendrick, F.; Chance, K.; Li, J.; Zheng, J.; Zhao, Y. Adjoint Inversion of Chinese Non-Methane Volatile Organic Compound Emissions Using Space-Based Observations of Formaldehyde and Glyoxal. *Atmospheric Chemistry and Physics* **2018**, *18* (20), 15017–15046.
- (32) Millet, D. B.; Jacob, D. J.; Boersma, K. F.; Fu, T.-M.; Kurosu, T. P.; Chance, K.; Heald, C. L.; Guenther, A. Spatial Distribution of Isoprene Emissions from North America Derived from Formaldehyde Column Measurements by the OMI Satellite Sensor. *J. Geophys. Res.* **2008**, *113* (D2), No. D02307.
- (33) Marais, E. A.; Jacob, D. J.; Kurosu, T. P.; Chance, K.; Murphy, J. G.; Reeves, C.; Mills, G.; Casadio, S.; Millet, D. B.; Barkley, M. P.; Paulot, F.; Mao, J. Isoprene Emissions in Africa Inferred from OMI Observations of Formaldehyde Columns. *Atmospheric Chemistry and Physics* **2012**, *12* (14), 6219–6235.
- (34) Gonzi, S.; Palmer, P. I.; Barkley, M. P.; De Smedt, I.; Van Roozendael, M. Biomass Burning Emission Estimates Inferred from Satellite Column Measurements of HCHO: Sensitivity to Co-emitted Aerosol and Injection Height. *Geophys. Res. Lett.* **2011**, *38* (14), n/a–n/a.
- (35) Sillman, S. The Use of NO_y, H₂O₂, and HNO₃ as Indicators for Ozone-NO_x-Hydrocarbon Sensitivity in Urban Locations. *J. Geophys. Res.* **1995**, *100* (D7), 14175.
- (36) Tonnesen, G. S.; Dennis, R. L. Analysis of Radical Propagation Efficiency to Assess Ozone Sensitivity to Hydrocarbons and NO_x: 2. Long-lived Species as Indicators of Ozone Concentration Sensitivity. *J. Geophys. Res. Atmospheres* **2000**, *105* (D7), 9227–9241.
- (37) Jin, X.; Holloway, T. Spatial and Temporal Variability of Ozone Sensitivity over China Observed from the Ozone Monitoring Instrument. *Journal of Geophysical Research: Atmospheres* **2015**, *120* (14), 7229–7246.
- (38) Jin, X.; Fiore, A. M.; Murray, L. T.; Valin, L. C.; Lamsal, L. N.; Duncan, B.; Folkert Boersma, K.; De Smedt, I.; Abad, G. G.; Chance, K.; Tonnesen, G. S. Evaluating a Space-Based Indicator of Surface Ozone-NO_x-VOC Sensitivity Over Midlatitude Source Regions and Application to Decadal Trends. *Journal of Geophysical Research: Atmospheres* **2017**, *122* (19), 10439.
- (39) Duncan, B. N.; Yoshida, Y.; Olson, J. R.; Sillman, S.; Martin, R. V.; Lamsal, L.; Hu, Y.; Pickering, K. E.; Allen, D. J.; Retscher, C.; Crawford, J. H. Application of OMI Observations to a Space-Based Indicator of NO_x and VOC Controls on Surface Ozone Formation. *Atmos. Environ.* **2010**, *44* (18), 2213–2223.
- (40) Goldberg, D. L.; Lu, Z.; Streets, D. G.; de Foy, B.; Griffin, D.; McLinden, C. A.; Lamsal, L. N.; Krotkov, N. A.; Eskes, H. Enhanced Capabilities of TROPOMI NO₂: Estimating NO_x from North American Cities and Power Plants. *Environ. Sci. Technol.* **2019**, *53* (21), 12594–12601.
- (41) Alvarado, L. M. A.; Richter, A.; Vrekoussis, M.; Hilboll, A.; Hedegaard, A. B. K.; Schneising, O.; Burrows, J. P. Unexpected Long-Range Transport of Glyoxal and Formaldehyde Observed from the Copernicus Sentinel-5 Precursor Satellite during the 2018 Canadian Wildfires. *Atmos. Chem. Phys.* **2020**, *20* (4), 2057–2072.
- (42) Lin, J.-T.; Martin, R. V.; Boersma, K. F.; Sneep, M.; Stammes, P.; Spurr, R.; Wang, P.; Van Roozendael, M.; Clemer, K.; Irie, H. Retrieving Tropospheric Nitrogen Dioxide from the Ozone Monitoring Instrument: Effects of Aerosols, Surface Reflectance Anisotropy, and Vertical Profile of Nitrogen Dioxide. *Atmospheric Chemistry and Physics* **2014**, *14* (3), 1441–1461.
- (43) Bouscerez, N. Space-Based Retrieval of NO₂ over Biomass Burning Regions: Quantifying and Reducing Uncertainties. *Atmospheric Measurement Techniques* **2014**, *7* (10), 3431–3444.
- (44) Boersma, K. F.; Eskes, H. J.; Richter, A.; De Smedt, I.; Lorente, A.; Beirle, S.; van Geffen, J. H. G. M.; Zara, M.; Peters, E.; Van Roozendael, M.; Wagner, T.; Maasakkers, J. D.; van der A, R. J.; Nightingale, J.; De Rudder, A.; Irie, H.; Pinardi, G.; Lambert, J.-C.; Compernolle, S. C. Improving Algorithms and Uncertainty Estimates for Satellite NO₂ retrievals: Results from the Quality Assurance for the Essential Climate Variables (QA4ECV) Project. *Atmospheric Measurement Techniques* **2018**, *11* (12), 6651–6678.
- (45) De Smedt, I.; Theys, N.; Yu, H.; Danckaert, T.; Lerot, C.; Compernolle, S.; Van Roozendael, M.; Richter, A.; Hilboll, A.; Peters, E.; Pedernana, M.; Loyola, D.; Beirle, S.; Wagner, T.; Eskes, H.; van Geffen, J.; Boersma, K. F.; Veefkind, P. Algorithm Theoretical Baseline for Formaldehyde Retrievals from SSP TROPOMI and from the QA4ECV Project. *Atmospheric Measurement Techniques* **2018**, *11* (4), 2395–2426.
- (46) Laughner, J. L.; Zhu, Q.; Cohen, R. C. The Berkeley High Resolution Tropospheric NO₂ Product. *Earth Syst. Sci. Data* **2018**, *10* (4), 2069–2095.
- (47) Goldberg, D. L.; Lamsal, L. N.; Loughner, C. P.; Swartz, W. H.; Lu, Z.; Streets, D. G. A High-Resolution and Observationally Constrained OMI NO₂ Satellite Retrieval. *Atmos. Chem. Phys.* **2017**, *17* (18), 11403–11421.
- (48) Russell, A. R.; Perring, A. E.; Valin, L. C.; Bucsela, E. J.; Browne, E. C.; Wooldridge, P. J.; Cohen, R. C. A High Spatial Resolution Retrieval of NO₂ Column Densities from OMI: Method and Evaluation. *Atmos. Chem. Phys.* **2011**, *11*, 8543–8554.
- (49) Laughner, J. L.; Zare, A.; Cohen, R. C. Effects of Daily Meteorology on the Interpretation of Space-Based Remote Sensing of NO₂. *Atmospheric Chemistry and Physics* **2016**, *16* (23), 15247–15264.
- (50) Mebust, A. K.; Cohen, R. C. Space-Based Observations of Fire NO_x Emission Coefficients: A Global Biome-Scale Comparison. *Atmospheric Chemistry and Physics* **2014**, *14* (5), 2509–2524.
- (51) Bey, I.; Jacob, D. J.; Yantosca, R. M.; Logan, J. A.; Field, B. D.; Fiore, A. M.; Li, Q.; Liu, H. Y.; Mickley, L. J.; Schultz, M. G. Global Modeling of Tropospheric Chemistry with Assimilated Meteorology: Model Description and Evaluation. *J. Geophys. Res. Atmospheres* **2001**, *106* (D19), 23073–23095.
- (52) Chen, D.; Wang, Y.; McElroy, M. B.; He, K.; Yantosca, R. M.; Le Sager, P. Regional CO Pollution and Export in China Simulated by the High-Resolution Nested-Grid GEOS-Chem Model. *Atmos. Chem. Phys.* **2009**, *9* (11), 3825–3839.
- (53) Travis, K. R.; Jacob, D. J.; Fisher, J. A.; Kim, P. S.; Marais, E. A.; Zhu, L.; Yu, K.; Miller, C. C.; Yantosca, R. M.; Sulprizio, M. P.; Thompson, A. M.; Wennberg, P. O.; Crounse, J. D.; St. Clair, J. M.; Cohen, R. C.; Laughner, J. L.; Dibb, J. E.; Hall, S. R.; Ullmann, K.; Wolfe, G. M.; Pollack, I. B.; Peischl, J.; Neuman, J. A.; Zhou, X. Why Do Models Overestimate Surface Ozone in the Southeast United States? *Atmospheric Chemistry and Physics* **2016**, *16* (21), 13561–13577.
- (54) Fisher, J. A.; Jacob, D. J.; Travis, K. R.; Kim, P. S.; Marais, E. A.; Chan Miller, C.; Yu, K.; Zhu, L.; Yantosca, R. M.; Sulprizio, M. P.; Mao, J.; Wennberg, P. O.; Crounse, J. D.; Teng, A. P.; Nguyen, T. B.; St. Clair, J. M.; Cohen, R. C.; Romer, P.; Nault, B. A.; Wooldridge, P. J.; Jimenez, J. L.; Campuzano-Jost, P.; Day, D. A.; Hu, W.; Shepson, P. B.; Xiong, F.; Blake, D. R.; Goldstein, A. H.; Misztal, P. K.; Hanisco, T. F.; Wolfe, G. M.; Ryerson, T. B.; Wisthaler, A.; Mikoviny, T. Organic Nitrate Chemistry and Its Implications for Nitrogen Budgets in an Isoprene- and Monoterpene-Rich Atmosphere: Constraints from Aircraft (SEAC4RS) and Ground-Based (SOAS) Observations in the Southeast US. *Atmos. Chem. Phys.* **2016**, *16* (9), 5969–5991.
- (55) van der Werf, G. R.; Randerson, J. T.; Giglio, L.; van Leeuwen, T. T.; Chen, Y.; Rogers, B. M.; Mu, M.; van Marle, M. J. E.; Morton, D. C.; Collatz, G. J.; Yokelson, R. J.; Kasibhatla, P. S. Global Fire Emissions Estimates during 1997–2016. *Earth System Science Data* **2017**, *9* (2), 697–720.

- (56) Giglio, L.; Randerson, J. T.; van der Werf, G. R. Analysis of Daily, Monthly, and Annual Burned Area Using the Fourth-generation Global Fire Emissions Database (GFED4). *J. Geophys. Res. Biogeosciences* **2013**, *118* (1), 317–328.
- (57) van der Werf, G. R.; Randerson, J. T.; Giglio, L.; Collatz, G. J.; Mu, M.; Kasibhatla, P. S.; Morton, D. C.; DeFries, R. S.; Jin, Y.; van Leeuwen, T. T. Global Fire Emissions and the Contribution of Deforestation, Savanna, Forest, Agricultural, and Peat Fires (1997–2009). *Atmospheric Chemistry and Physics* **2010**, *10* (23), 11707–11735.
- (58) Akagi, S. K.; Yokelson, R. J.; Wiedinmyer, C.; Alvarado, M. J.; Reid, J. S.; Karl, T.; Crounse, J. D.; Wennberg, P. O. Emission Factors for Open and Domestic Biomass Burning for Use in Atmospheric Models. *Atmospheric Chemistry and Physics* **2011**, *11* (9), 4039–4072.
- (59) Fischer, E. V.; Jacob, D. J.; Yantosca, R. M.; Sulprizio, M. P.; Millet, D. B.; Mao, J.; Paulot, F.; Singh, H. B.; Roiger, A.; Ries, L.; Talbot, R. W.; Dzepina, K.; Deolal, S. P. Atmospheric Peroxyacetyl Nitrate (PAN): A Global Budget and Source Attribution. *Atmospheric Chemistry and Physics* **2014**, *14* (5), 2679–2698.
- (60) Carter, T. S.; Heald, C. L.; Kroll, J. H.; Apel, E. C.; Blake, D.; Coggon, M.; Edtbauer, A.; Gkatzelis, G.; Hornbrook, R. S.; Peischl, J.; Pfannerstill, E. Y.; Piel, F.; Reijrink, N. G.; Ringsdorf, A.; Warneke, C.; Williams, J.; Wisthaler, A.; Xu, L. An Improved Representation of Fire Non-Methane Organic Gases (NMOGs) in Models: Emissions to Reactivity. *Atmos. Chem. Phys.* **2022**, *22* (18), 12093–12111.
- (61) Kwon, H.-A.; Park, R. J.; Oak, Y. J.; Nowlan, C. R.; Janz, S. J.; Kowalewski, M. G.; Fried, A.; Walega, J.; Bates, K. H.; Choi, J.; Blake, D. R.; Wisthaler, A.; Woo, J.-H. Top-down Estimates of Anthropogenic VOC Emissions in South Korea Using Formaldehyde Vertical Column Densities from Aircraft during the KORUS-AQ Campaign. *Elementa Sci. Anthropocene* **2021**, *9* (1). DOI: [10.1525/elementa.2021.00109](https://doi.org/10.1525/elementa.2021.00109).
- (62) Palmer, P. I.; Jacob, D. J.; Chance, K.; Martin, R. V.; Spurr, R. J. D.; Kurosu, T. P.; Bey, I.; Yantosca, R.; Fiore, A.; Li, Q. Air Mass Factor Formulation for Spectroscopic Measurements from Satellites: Application to Formaldehyde Retrievals from the Global Ozone Monitoring Experiment. *J. Geophys. Res. Atmospheres* **2001**, *106* (D13), 14539–14550.
- (63) Spurr, R. *LIDORT and VLIDORT: Linearized Pseudo-Spherical Scalar and Vector Discrete Ordinate Radiative Transfer Models for Use in Remote Sensing Retrieval Problems; Light Scattering Reviews* **3** *2008*, 229–275.
- (64) Martin, R. V.; Chance, K.; Jacob, D. J.; Kurosu, T. P.; Spurr, R. J. D.; Bussela, E.; Gleason, J. F.; Palmer, P. I.; Bey, I.; Fiore, A. M.; Li, Q.; Yantosca, R. M.; Koelemeijer, R. B. A. An Improved Retrieval of Tropospheric Nitrogen Dioxide from GOME. *J. Geophys. Res. Atmospheres* **2002**, *107* (D20), ACH 9-1–ACH 9-21.
- (65) Vasilkov, A.; Krotkov, N.; Yang, E.-S.; Lamsal, L.; Joiner, J.; Castellanos, P.; Fasnacht, Z.; Spurr, R. Explicit and Consistent Aerosol Correction for Visible Wavelength Satellite Cloud and Nitrogen Dioxide Retrievals Based on Optical Properties from a Global Aerosol Analysis. *Atmos. Meas. Technol.* **2021**, *14* (4), 2857–2871.
- (66) Griffin, D.; McLinden, C. A.; Dammers, E.; Adams, C.; Stockwell, C. E.; Warneke, C.; Bourgeois, I.; Peischl, J.; Ryerson, T. B.; Zarzana, K. J.; Rowe, J. P.; Volkamer, R.; Knote, C.; Kille, N.; Koenig, T. K.; Lee, C. F.; Rollins, D.; Rickly, P. S.; Chen, J.; Fehr, L.; Bourassa, A.; Degenstein, D.; Hayden, K.; Mihele, C.; Wren, S. N.; Liggio, J.; Akingunola, A.; Makar, P. Biomass Burning Nitrogen Dioxide Emissions Derived from Space with TROPOMI: Methodology and Validation. *Atmos. Meas. Technol.* **2021**, *14* (12), 7929–7957.
- (67) NOAA. Hazard Mapping System Fire and Smoke Product. <https://www.ospo.noaa.gov/Products/land/hms.html#0> (accessed 2023-05-12).
- (68) Rolph, G. D.; Draxler, R. R.; Stein, A. F.; Taylor, A.; Ruminski, M. G.; Kondragunta, S.; Zeng, J.; Huang, H.-C.; Manikin, G.; McQueen, J. T.; Davidson, P. M. Description and Verification of the NOAA Smoke Forecasting System: The 2007 Fire Season. *Weather Forecast* **2009**, *24* (2), 361–378.
- (69) O'Dell, K.; Ford, B.; Fischer, E. V.; Pierce, J. R. Contribution of Wildland-Fire Smoke to US PM 2.5 and Its Influence on Recent Trends. *Environ. Sci. Technol.* **2019**, *S3* (4), 1797–1804.
- (70) Childs, M. L.; Li, J.; Wen, J.; Heft-Neal, S.; Driscoll, A.; Wang, S.; Gould, C. F.; Qiu, M.; Burney, J.; Burke, M. Daily Local-Level Estimates of Ambient Wildfire Smoke PM_{2.5} for the Contiguous US. *Environ. Sci. Technol.* **2022**, *S6* (19), 13607–13621.
- (71) Brey, S. J.; Fischer, E. V. Smoke in the City: How Often and Where Does Smoke Impact Summertime Ozone in the United States? *Environ. Sci. Technol.* **2016**, *S0* (3), 1288–1294.
- (72) O'Dell, K.; Hornbrook, R. S.; Permar, W.; Levin, E. J. T.; Garofalo, L. A.; Apel, E. C.; Blake, N. J.; Jarnot, A.; Pothier, M. A.; Farmer, D. K.; Hu, L.; Campos, T.; Ford, B.; Pierce, J. R.; Fischer, E. V. Hazardous Air Pollutants in Fresh and Aged Western US Wildfire Smoke and Implications for Long-Term Exposure. *Environ. Sci. Technol.* **2020**, *S4* (19), 11838–11847.
- (73) Giglio, L.; Schroeder, W.; Justice, C. O. The Collection 6 MODIS Active Fire Detection Algorithm and Fire Products. *Remote Sens Environ* **2016**, *178*, 31–41.
- (74) MODIS Collection 6 Hotspot/Active Fire Detections MCD14 ML distributed from NASA FIRMS. DOI: [10.5067/FIRMS/MODIS/MCD14ML](https://doi.org/10.5067/FIRMS/MODIS/MCD14ML).
- (75) Stein, A. F.; Draxler, R. R.; Rolph, G. D.; Stunder, B. J. B.; Cohen, M. D.; Ngan, F. NOAA's HYSPLIT Atmospheric Transport and Dispersion Modeling System. *B Am. Meteorol Soc.* **2015**, *96*, 2059–2077.
- (76) Stunder, B. J. B.; Cohen, M. D.; Ngan, F.; Stein, A. F.; Draxler, R. R.; Rolph, G. D. NOAA's HYSPLIT Atmospheric Transport and Dispersion Modeling System. *Bulletin of the American Meteorological Society* **2015**, *96* (12), 2059–2077.
- (77) Mesinger, F.; DiMego, G.; Kalnay, E.; Mitchell, K.; Shafran, P. C.; Ebisuzaki, W.; Jović, D.; Woollen, J.; Rogers, E.; Berbery, E. H.; Ek, M. B.; Fan, Y.; Grumbine, R.; Higgins, W.; Li, H.; Lin, Y.; Manikin, G.; Parrish, D.; Shi, W. North American Regional Reanalysis. *B Am. Meteorol Soc.* **2006**, *87* (3), 343–360.
- (78) Jin, X. Observing the Distributions and Chemistry of Major Air Pollutants (O_3 and PM_{2.5}) from Space: Trends, Uncertainties, and Health Implications. Ph.D. thesis, Columbia University ProQuest Dissertations Publishing, 2020. DOI: [10.7916/d8-cxn5-h474](https://doi.org/10.7916/d8-cxn5-h474).
- (79) Farmer, D. K.; Perring, A. E.; Wooldridge, P. J.; Blake, D. R.; Baker, A.; Meinardi, S.; Huey, L. G.; Tanner, D.; Vargas, O.; Cohen, R. C. Impact of Organic Nitrates on Urban Ozone Production. *Atmospheric Chemistry and Physics* **2011**, *11* (9), 4085–4094.
- (80) Murphy, J. G.; Day, D. A.; Cleary, P. A.; Wooldridge, P. J.; Millet, D. B.; Goldstein, A. H.; Cohen, R. C. The Weekend Effect within and Downwind of Sacramento - Part 1: Observations of Ozone, Nitrogen Oxides, and VOC Reactivity. *Atmospheric Chemistry and Physics* **2007**, *7* (20), 5327–5339.
- (81) Pusede, S. E.; Gentner, D. R.; Wooldridge, P. J.; Browne, E. C.; Rollins, A. W.; Min, K.-E.; Russell, A. R.; Thomas, J.; Zhang, L.; Brune, W. H.; Henry, S. B.; DiGangi, J. P.; Keutsch, F. N.; Harrold, S. A.; Thornton, J. A.; Beaver, M. R.; St. Clair, J. M.; Wennberg, P. O.; Sanders, J.; Ren, X.; VandenBoer, T. C.; Markovic, M. Z.; Guha, A.; Weber, R.; Goldstein, A. H.; Cohen, R. C. On the Temperature Dependence of Organic Reactivity, Nitrogen Oxides, Ozone Production, and the Impact of Emission Controls in San Joaquin Valley, California. *Atmospheric Chemistry and Physics* **2014**, *14* (7), 3373–3395.
- (82) Pusede, S. E.; Cohen, R. C. On the Observed Response of Ozone to NO_x and VOC Reactivity Reductions in San Joaquin Valley California 1995–Present. *Atmospheric Chemistry and Physics* **2012**, *12* (18), 8323–8339.
- (83) Williams, J. E.; Boersma, K. F.; Le Sager, P.; Verstraeten, W. W. The High-Resolution Version of TMS-MP for Optimized Satellite Retrievals: Description and Validation. *Geoscientific Model Development* **2017**, *10* (2), 721–750.

- (84) Lamsal, L. N.; Duncan, B. N.; Yoshida, Y.; Krotkov, N. A.; Pickering, K. E.; Streets, D. G.; Lu, Z. U.S. NO₂ Trends (2005–2013): EPA Air Quality System (AQS) Data versus Improved Observations from the Ozone Monitoring Instrument (OMI). *Atmos. Environ.* **2015**, *110* (C), 130–143.
- (85) Liu, F.; Page, A.; Strode, S. A.; Yoshida, Y.; Choi, S.; Zheng, B.; Lamsal, L. N.; Li, C.; Krotkov, N. A.; Eskes, H.; van der A, R.; Veefkind, P.; Levelt, P. F.; Hauser, O. P.; Joiner, J. Abrupt Decline in Tropospheric Nitrogen Dioxide over China after the Outbreak of COVID-19. *Sci. Adv.* **2020**, *6*, No. eabc2992.
- (86) Goldberg, D. L.; Anenberg, S. C.; Griffin, D.; McLinden, C. A.; Lu, Z.; Streets, D. G. Disentangling the Impact of the COVID-19 Lockdowns on Urban NO₂ From Natural Variability. *Geophys. Res. Lett.* **2020**, *47* (17), No. e2020GL089269.
- (87) Ninneman, M.; Jaffe, D. A. The Impact of Wildfire Smoke on Ozone Production in an Urban Area: Insights from Field Observations and Photochemical Box Modeling. *Atmos. Environ.* **2021**, *267*, No. 118764.
- (88) Valin, L. C.; Russell, A. R.; Hudman, R. C.; Cohen, R. C. Effects of Model Resolution on the Interpretation of Satellite NO₂ Observations. *Atmospheric Chemistry and Physics* **2011**, *11* (22), 11647–11655.
- (89) Calahorrano, J. F. J.; Lindaas, J.; O'Dell, K.; Palm, B. B.; Peng, Q.; Flocke, F.; Pollack, I. B.; Garofalo, L. A.; Farmer, D. K.; Pierce, J. R.; Collett, J. L.; Weinheimer, A.; Campos, T.; Hornbrook, R. S.; Hall, S. R.; Ullmann, K.; Pothier, M. A.; Apel, E. C.; Permar, W.; Hu, L.; Hills, A. J.; Montzka, D.; Tyndall, G.; Thornton, J. A.; Fischer, E. V. Daytime Oxidized Reactive Nitrogen Partitioning in Western U.S. Wildfire Smoke Plumes. *J. Geophys. Res. Atmospheres* **2021**, *126* (4). DOI: [10.1029/2020JD033484](https://doi.org/10.1029/2020JD033484).
- (90) Wolfe, G. M.; Kaiser, J.; Hanisco, T. F.; Keutsch, F. N.; de Gouw, J. A.; Gilman, J. B.; Graus, M.; Hatch, C. D.; Holloway, J.; Horowitz, L. W.; Lee, B. H.; Lerner, B. M.; Lopez-Hilfiker, F.; Mao, J.; Marvin, M. R.; Peischl, J.; Pollack, I. B.; Roberts, J. M.; Ryerson, T. B.; Thornton, J. A.; Veres, P. R.; Warneke, C. Formaldehyde Production from Isoprene Oxidation across NO_x Regimes. *Atmospheric Chemistry and Physics* **2016**, *16* (4), 2597–2610.
- (91) Saunders, S. M.; Jenkin, M. E.; Derwent, R. G.; Pilling, M. J. Protocol for the Development of the Master Chemical Mechanism, MCM v3 (Part A): Tropospheric Degradation of Non-Aromatic Volatile Organic Compounds. *Atmos. Chem. Phys.* **2003**, *3* (1), 161–180.
- (92) Jenkin, M. E.; Saunders, S. M.; Pilling, M. J. The Tropospheric Degradation of Volatile Organic Compounds: A Protocol for Mechanism Development. *Atmos. Environ.* **1997**, *31* (1), 81–104.
- (93) Jenkin, M. E.; Young, J. C.; Rickard, A. R. The MCM v3.3.1 Degradation Scheme for Isoprene. *Atmos. Chem. Phys.* **2015**, *15* (20), 11433–11459.
- (94) Zhu, L.; Jacob, D. J.; Keutsch, F. N.; Mickley, L. J.; Scheffe, R.; Strum, M.; Abad, G. G.; Chance, K.; Yang, K.; Rappenglück, B.; Millet, D. B.; Baasandorj, M.; Jaeglé, L.; Shah, V. Formaldehyde (HCHO) As a Hazardous Air Pollutant: Mapping Surface Air Concentrations from Satellite and Inferring Cancer Risks in the United States. *Environ. Sci. Technol.* **2017**, *51* (10), S650–S657.
- (95) Martin, R. V.; Fiore, A. M.; Van Donkelaar, A. Space-Based Diagnosis of Surface Ozone Sensitivity to Anthropogenic Emissions. *Geophys. Res. Lett.* **2004**, *31* (6), No. L06120.
- (96) Friedl, M. A.; Sulla-Menashe, D.; Tan, B.; Schneider, A.; Ramankutty, N.; Sibley, A.; Huang, X. MODIS Collection 5 global land cover: Algorithm refinements and characterization of new datasets. *Remote Sensing of Environment* **2010**, *114*, 168–182.
- (97) Kleinman, L. I.; Daum, P. H.; Lee, Y.; Nunnermacker, L. J.; Springer, S. R.; Weinstein-Lloyd, J.; Rudolph, J. Ozone Production Efficiency in an Urban Area. *J. Geophys. Res. Atmospheres* **1984** **2012** *2002*, *107* (D23), ACH 23-1–ACH 23-12.
- (98) Sillman, S. The Relation between Ozone, NO_x and Hydrocarbons in Urban and Polluted Rural Environments. *Atmos. Environ.* **1999**, *33* (12), 1821–1845.
- (99) Wang, S.; Coggon, M. M.; Gkatzelis, G. I.; Warneke, C.; Bourgeois, I.; Ryerson, T.; Peischl, J.; Veres, P. R.; Neuman, J. A.; Hair, J.; Shingler, T.; Fenn, M.; Diskin, G.; Huey, L. G.; Lee, Y. R.; Apel, E. C.; Hornbrook, R. S.; Hills, A. J.; Hall, S. R.; Ullmann, K.; Bela, M. M.; Trainer, M. K.; Kumar, R.; Orlando, J. J.; Flocke, F. M.; Emmons, L. K. Chemical Tomography in a Fresh Wildland Fire Plume: A Large Eddy Simulation (LES) Study. *J. Geophys. Res.: Atmos.* **2021**, *126* (18). DOI: [10.1029/2021JD035203](https://doi.org/10.1029/2021JD035203).
- (100) Jaffe, D. A.; Wigder, N. L. Ozone Production from Wildfires: A Critical Review. *Atmos. Environ.* **2012**, *51* (C), 1–10.
- (101) Baylon, P.; Jaffe, D. A.; Hall, S. R.; Ullmann, K.; Alvarado, M. J.; Lefer, B. L. Impact of Biomass Burning Plumes on Photolysis Rates and Ozone Formation at the Mount Bachelor Observatory. *Journal of Geophysical Research: Atmospheres* **2018**, *123* (4), 2272–2284.
- (102) Ivatt, P. D.; Evans, M. J.; Lewis, A. C. Suppression of Surface Ozone by an Aerosol-Inhibited Photochemical Ozone Regime. *Nat. Geosci.* **2022**, *15* (7), 536–540.
- (103) Peng, Q.; Palm, B. B.; Melander, K. E.; Lee, B. H.; Hall, S. R.; Ullmann, K.; Campos, T.; Weinheimer, A. J.; Apel, E. C.; Hornbrook, R. S.; Hills, A. J.; Montzka, D. D.; Flocke, F.; Hu, L.; Permar, W.; Wielgasz, C.; Lindaas, J.; Pollack, I. B.; Fischer, E. V.; Bertram, T. H.; Thornton, J. A. HONO Emissions from Western U.S. Wildfires Provide Dominant Radical Source in Fresh Wildfire Smoke. *Environ. Sci. Technol.* **2020**, *54* (10), 5954–5963.
- (104) Zhu, L.; Val Martin, M.; Gatti, L. V.; Kahn, R.; Hecobian, A.; Fischer, E. V. Development and Implementation of a New Biomass Burning Emissions Injection Height Scheme (BBEIH v1.0) for the GEOS-Chem Model (v9-01-01). *Geosci. Model Dev.* **2018**, *11* (10), 4103–4116.
- (105) Chance, K.; Liu, X.; Suleiman, R. M.; Flittner, D. E.; Al-Saadi, J.; Janz, S. J. Tropospheric Emissions: Monitoring of Pollution (TEMPO). *SPIE Optical* **2013**, No. 88660D.